

# Analysis of the deformation of gel-spun polyethylene fibres using Raman spectroscopy

W. F. WONG, R. J. YOUNG

*Polymer Science and Technology Group, Manchester Materials Science Centre, UMIST/University of Manchester, Manchester M60 1QD, UK*

Raman spectroscopy has been used to investigate molecular deformation in a number of high-performance gel-spun polyethylene (PE) fibres. Well-defined Raman spectra can be obtained for the fibres and the study has concentrated upon the symmetric C–C stretching mode ( $1128\text{ cm}^{-1}$ ). During mechanical deformation, the Raman spectra show the existence of a bimodal molecular stress distribution in the crystalline phase resulting in splitting of the Raman band. The changes in the Raman band peak position and area with strain for different modes of deformation, including stress relaxation and creep, have indicated the molecular response of the material to stress is highly complicated. This information, however, is particularly useful in analysing the molecular deformation both quantitatively and qualitatively and it is shown that the Young's modulus of the fibres is related to both the relative areas of the two Raman bands and their rate of shift per unit strain.

## 1. Introduction

High-performance gel-spun ultra-high molecular weight polyethylene (UHMW-PE) fibres, with Young's moduli of 100–200 GPa and tensile strengths of 2–5 GPa [1–6] are superior to classical materials such as steel on a property–weight basis. It is of considerable interest to know what aspects of the structure give such good mechanical properties and to know what mechanisms or defects cause the properties to fall below their theoretical predictions. Calculations have shown that the theoretical modulus of linear PE could be about 300 GPa with a strength of 19–36 GPa [7, 8].

Raman spectroscopy has been proved to be a successful technique to study the deformation of high-performance fibres, particularly in a monofilament form, at the molecular level [9–22]. It provides an important insight into the response of molecules in the fibres to various modes of deformation. When such polymers are deformed the bonds in the molecular backbone are strained and some of the frequencies of Raman-active bands shift to lower wave numbers. In PE, well-defined Raman spectra can be obtained and stress-induced band frequency shifts are observed [18–22]. Kip *et al.* [20] studied the molecular deformation of gel-spun UHMW-PE by Raman microscopy and found that both the asymmetric ( $1059\text{ cm}^{-1}$ ) and symmetric ( $1127\text{ cm}^{-1}$ ) C–C stretching modes demonstrated well-defined band splitting and a bimodal load distribution (with both low-load and high-load-bearing C–C bonds) upon stretching. They analysed these two components by fitting the peaks in the Raman spectra to two Gaussian curves and this enabled them to study the different behaviour of each component upon deformation. Continuing the

work on gel-spun UHMW-PE fibres, Moonen *et al.* [21] and Grubb and Li [22] have demonstrated that an intense high-load-bearing peak could be obtained for both the asymmetric ( $1059\text{ cm}^{-1}$ ) and symmetric ( $1127\text{ cm}^{-1}$ ) C–C stretching modes at low temperature ( $< 240\text{ K}$ ) where stress relaxation was suppressed. According to both groups [21, 22], the two components in the fibre structure are crystalline with one of them inefficiently coupled to the applied stress and carrying little load upon straining.

## 2. Experimental procedure

### 2.1. Materials

The fibres used in this work included both commercial (Fibres A and B) and experimental (Fibres C–I) PE fibres as shown in Table I. Intrinsic viscosity values are also listed in Table I for all the experimental fibres [23]. The commercial Spectra 1000 and all the experimental PE fibres are all gel-spun UHMW-PE fibres and were provided by Allied-Signal Inc., while the commercial melt-spun Snia fibre was obtained from DRA, Farnborough. This work has concentrated principally upon the gel-spun Spectra 1000 fibre (Fibre A), the melt-spun Snia fibre (Fibre B) and the experimental gel-spun PE fibre (Fibre C). Snia is a commercial melt-spun conventional PE fibre which was used for comparison purpose and the experimental gel-spun Fibre C was investigated in detail because it has been found to have the highest value of modulus among the fibres investigated [23]. The fibres were all found to have similar degrees of molecular alignment as determined by X-ray diffraction [23].

TABLE I Details of the commercial and experimental samples of UHMW-PE fibres studied

Fibre	Sample/code	Diameter ( $\mu\text{m}$ )	Intrinsic viscosity ( $\text{dl g}^{-1}$ )	$T_m$ ( $^{\circ}\text{C}$ )	$\Delta H_f$ ( $\text{J g}^{-1}$ )	$\phi_c$ (%)
A	Spectra 1000	$26.0 \pm 4.5$	–	147.5	273.3	92.5
B	Snia	$15.3 \pm 2.5$	–	141.5	267.3	90.5
C	Experimental	$14.3 \pm 1.2$	18	145.6	284.5	96.3
D	Experimental	$27.4 \pm 1.2$	18	145.0	266.5	90.2
E	Experimental	$29.8 \pm 2.7$	18	142.4	264.9	89.6
F	Experimental	$23.8 \pm 1.8$	18	144.5	262.7	88.9
G	Experimental	$15.1 \pm 2.5$	7	144.7	262.2	88.7
H	Experimental	$21.6 \pm 2.5$	11	144.2	268.3	90.8
I	Experimental	$27.8 \pm 6.4$	18	132.7	259.0	87.6

## 2.2. Mechanical testing

Stress–strain measurements were carried out for all the fibres. Individual monofilaments of PE fibres were mounted across a hole in a paper card using Ciba-Geigy HY/LY 1927 two-part solvent-free cold-setting epoxy resin. The card was then mounted between fibre testing grips in a model 1211 Instron tensile tester and the card edges were cut. A 5 N capacity load was used with the scale calibrated at its maximum load. Significant end effects are generally found in highly oriented polymers due to the insufficiently long gauge lengths [24]. As a result, samples of different gauge lengths were tested at a constant strain rate of  $1.67 \times 10^{-3} \text{ s}^{-1}$  to determine the corrected values of modulus and strength by extrapolating the values to infinite and zero gauge lengths, respectively. All the mechanical testing was carried out at  $23 \pm 1^{\circ}\text{C}$  and a relative humidity of  $50\% \pm 2\%$ .

## 2.3. Structural characterization

A Joel field-emission scanning electron microscope (FE-SEM, model JSM6300) operated at 2–3 kV was used to examine the monofilaments both externally and internally. This was found to be considerably better than a conventional SEM, producing high-resolution micrographs at low voltage. To reveal the internal microstructure of the monofilaments, it was necessary to prepare the specimens by longitudinal splitting of the monofilaments at room temperature. Replicas of the internal surfaces of the split monofilaments were obtained in order to examine the microstructure by transmission electron microscopy (TEM). The replicas were prepared by etching the monofilaments using permanganic acid [25] to reveal the crystalline microstructure, followed by two-stage replication using cellulose acetate sheets.

The melting point,  $T_m$ , and enthalpies of fusion,  $\Delta H_f$ , of the fibres (Table I) were both determined under nitrogen by using a Du Pont 2000 heat-flux differential scanning calorimetry (DSC) at a scan speed of  $5^{\circ}\text{C min}^{-1}$ . The instrument was calibrated for temperature using both tin and indium, while indium was used as a standard for the calibration of the enthalpy of fusion. The value of the degree of crystallinity,  $\phi_c$ , was calculated from  $\Delta H_f$  by taking an average value for the enthalpy of fusion of those

quoted for orthorhombic PE crystals, i.e.  $295.5 \text{ J g}^{-1}$  [26].

## 2.4. Raman spectroscopy

Raman spectra were obtained at temperature of  $20 \pm 2^{\circ}\text{C}$  from individual PE monofilaments during deformation in a Raman microprobe system. This is based upon a SPEX 1403 double monochromator connected to a modified Nikon optical microscope. A  $\times 40$  objective lens with a numerical aperture of 0.65 was used and this gave a  $\sim 2 \mu\text{m}$  spot with the power of 1.5 mW when focused. The spectra were obtained using the 488.0 nm line of a 15 mW argon ion laser and the laser beam was polarized parallel to the fibre axis. The spectra were collected using a highly-sensitive Wright Instruments liquid-nitrogen cooled Charge Coupled Device (CCD) camera and analysed using the AT1 software supplied with the instrument. This silicon-based CCD detector has proven to be very effective for the detection of Raman scattering [27] and enabled relatively short exposure times (50 s) to be used for all the measurements. This is significant when compared with the conventional diode array detectors used by Moonen *et al.* [21] and Grubb and Li [22] for their Raman experiments in which the exposure times were more than 3 min. They had to resort to low temperature ( $\sim 240 \text{ K}$ ) measurements to avoid problems with stress relaxation during their Raman experiments.

The individual monofilaments were mounted across a hole on paper card using the Ciba-Geigy LY/HY 1927 two-part solvent-free cold-setting epoxy resin. The card was then mounted on to the aluminium blocks of the straining rig and the card edges were cut. The straining rig was equipped with a 5 N load cell and was fitted directly on to the microscope stage. The monofilament was stretched by displacing the blocks using the micrometer attachment. Four different initial gauge lengths of 10.0, 15.0, 20.0 and 25.0 mm at a constant strain rate of  $1.33 \times 10^{-4} \text{ s}^{-1}$  were employed to avoid the similar end effects found in tensile testing. This allowed the corrected values of rates of Raman band shift ( $d\Delta\nu/de$ ) for the monofilaments to be determined by extrapolating to infinite gauge length. Stress relaxation at constant displacement and creep experiments at constant load were carried out with a

series of scans to obtain the Raman spectra over a period of time.

### 3. Results and discussion

#### 3.1. Mechanical properties and morphology

Fig. 1 shows the stress-strain curves of Fibres A, B and C for a gauge length of 50 mm and at the strain rate of  $1.67 \times 10^{-3} \text{ s}^{-1}$ . The stress-strain curves of these monofilaments are essentially non-linear with significant differences in mechanical properties between the monofilaments. Both the gel-spun fibres (Fibres A and C) have higher values of initial modulus and strength than the melt-spun Fibre B. The values of modulus and strength corrected for gauge length are tabulated for all the fibres in Table II and it appears that Fibre C has the highest values of modulus and strength of all the samples.

Fig. 2 shows the surface textures of the monofilaments of Fibres A, B and C obtained using FE-SEM. Although they have different mechanical properties (Table II), there appears to be no significant difference in surface morphology between the three fibres which have a uniform longitudinal continuity of

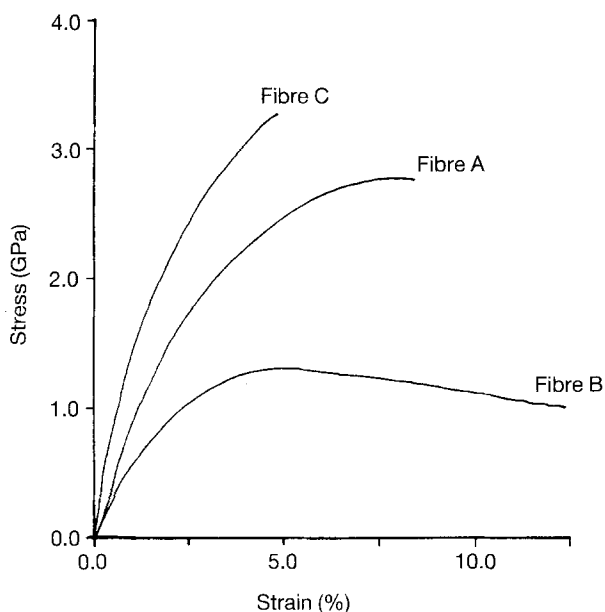


Figure 1 The stress-strain curves of Fibres A, B and C for a gauge length of 50.0 mm and a strain rate of  $1.67 \times 10^{-3} \text{ s}^{-1}$  at temperature  $23 \pm 1^\circ \text{C}$ .

TABLE II Modulus and strength values for the PE samples (corrected for gauge length) at strain rate of  $1.67 \times 10^3 \text{ s}^{-1}$

Fibre	Corrected modulus (GPa)	Corrected strength (GPa)
A	92	3.9
B	51	0.9
C	164	5.4
D	62	2.3
E	38	1.9
F	51	2.7
G	88	3.1
H	61	1.5
I	61	1.9

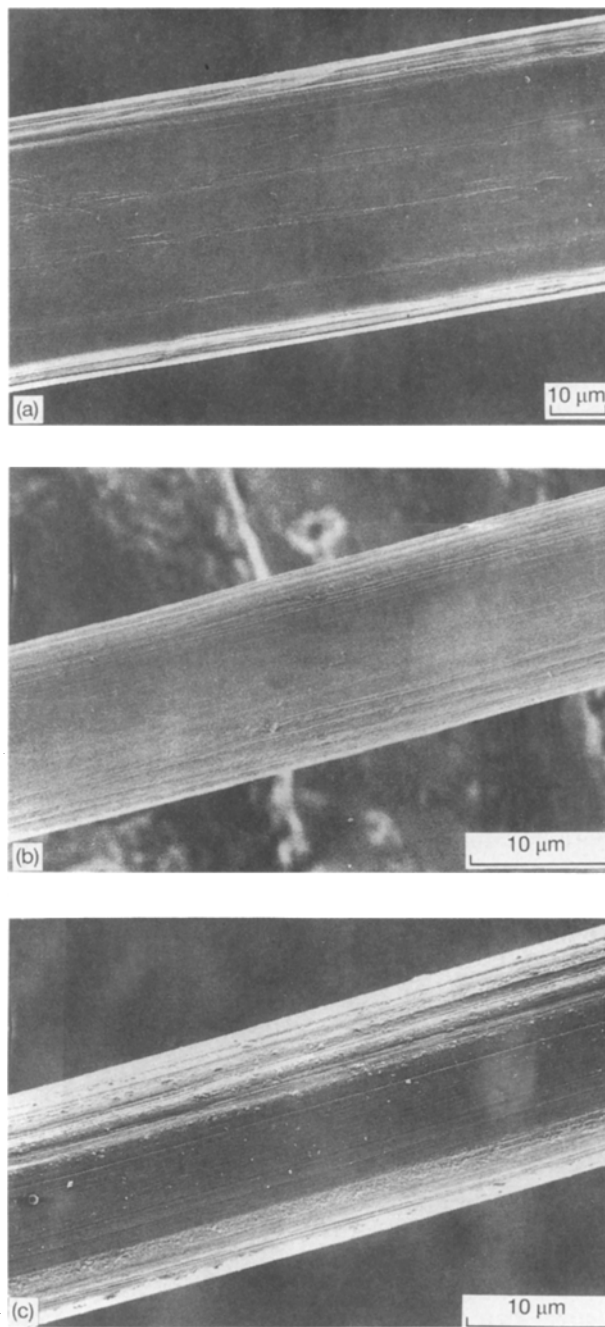


Figure 2 FE-SEM micrographs of the surface for the monofilaments of (a) Fibre A, (b) Fibre B, and (c) Fibre C.

the striations parallel to the fibre axis. Similar observations were obtained for the other experimental gel-spun PE fibres and these results suggest similarities of surface roughness and appearance between the gel-spun and melt-spun PE fibres. By performing longitudinal splitting of the monofilaments, the internal fibrillar microstructure of Fibres A, B and C can be seen clearly using FE-SEM as shown in Fig. 3. The monofilaments were seen to be composed mainly of fibrils which appear to be bundles of microfibrils. This is particularly obvious for the monofilaments of the gel-spun (UHMW-PE) Fibres A and C where the microfibrils (30–60 nm diameter) appear to be loosely entangled following splitting (Fig. 3a and c). The diameters of the fibrils are significantly different for the different fibres. The melt-spun Fibre B (Fig. 3b) has

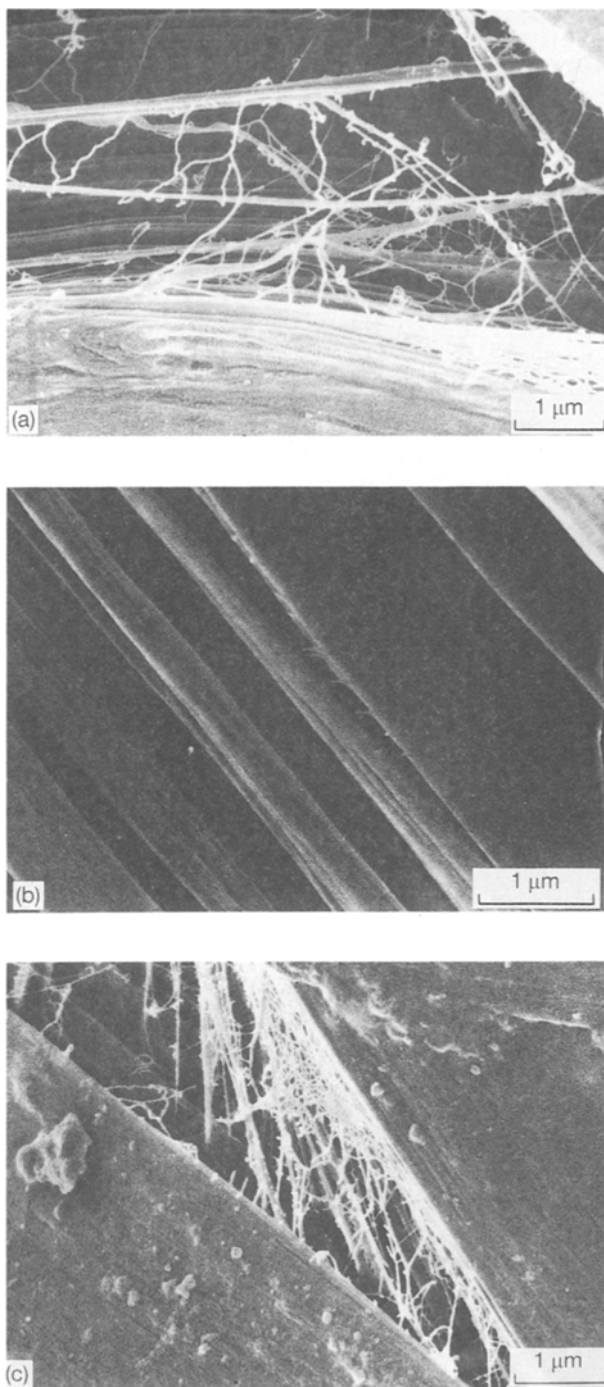


Figure 3 FE-SEM micrographs of the internal microstructures of the monofilaments of (a) Fibre A, (b) Fibre B, and (c) Fibre C.

the highest diameter fibrils ( $0.2\text{--}0.3\ \mu\text{m}$ ) which are about ten times larger than the microfibrils of the gel-spun Fibres A and C. This indicates that the two processing methods with different molar mass precursors produce different types of fibrillar structure in the PE fibres.

Fig. 4 shows the transmission electron micrographs for the replicas of etched sections of the monofilaments of Fibres A, B and C respectively. For Fibre A (Fig. 4a), the microfibrils are well oriented along the fibre axis which is consistent with the observation by FE-SEM. It was estimated that the microfibrils have a length of  $2\text{--}3\ \mu\text{m}$  with diameters of  $\sim 30\ \text{nm}$ . Such internal structure is similar to that of Fibre C as shown in Fig. 4c which appears to have an even more

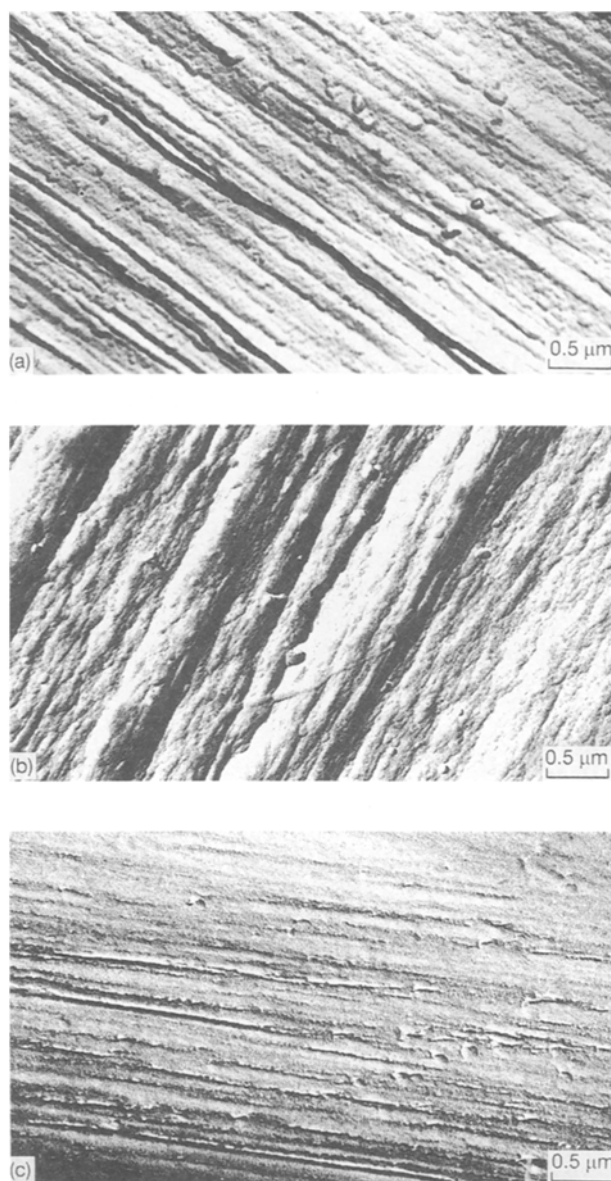


Figure 4 Transmission electron micrographs of the etched monofilaments of (a) Fibre A, (b) Fibre B, and (c) Fibre C.

well-defined microfibrillar microstructure. In contrast, the morphology of the melt-spun Fibre B (Fig. 4b) has an underlying fibrillar structure ( $0.2\text{--}0.4\ \mu\text{m}$  diameter) but the main morphology appears to be a block-like lamellar structure not found in the gel-spun fibres (Fig. 4a and c). It appears that the gel-spun PE fibres are more highly chain-extended than the melt-spun PE fibres.

### 3.2. Raman deformation measurements

The Raman spectra for the monofilaments of Fibres A, B and C in the range  $1070\text{--}1150\ \text{cm}^{-1}$  are presented in Fig. 5. They show the symmetric C–C stretching mode Raman band at  $1128\ \text{cm}^{-1}$ , together with the spectra after deformation to various strains. It can be seen that deformation results in well-defined band splitting for the gel-spun Fibres A and C (Fig. 5a and c) as found before [21, 22]. In contrast, the Raman band for the melt-spun Fibre B shows only a very small change upon deformation (Fig. 5b). In all cases the spectra can be fitted with a linear background to one narrow

curve and one broad Gaussian curve as illustrated in Fig. 6 for Fibre A. Fig. 6b shows that the band splits into two well-defined peaks and following Kip *et al.* [20], the narrow and broad peaks have been designated the “low-load” and “high-load” bearing bands, respectively. However, it has also been found in this present study that even the Raman band for the undeformed fibre can normally be fitted to two Gaussian curves with a different peak position (Fig. 6a). This observation is different from that of previous workers [21, 22] who suggested that the band splitting took place as a result of deformation and they did not consider any splitting for the bands in undeformed fibres. The slight asymmetry generally found for the band in the undeformed fibre can be accounted for by these two peaks. It was possible to optimize the fit of the two peaks to the Raman band using the AT1 software and generally the fit to two bands was found to be excellent for both deformed and undeformed Raman bands. As well as a shift in the frequency of the Raman band, it was found that both bands underwent significant broadening during defor-

mation as has been found for other fibres such as Kevlar [13–15].

Fig. 7 shows the typical dependence of the Raman band peak position,  $\Delta\nu$ , upon strain,  $e$ , for both the high-load- and low-load-bearing bands of Fibre A using a strain rate of  $1.33 \times 10^{-4} \text{ s}^{-1}$  and a gauge length of 25.0 mm. The observed change in peak position for both bands is approximately linear at low strains ( $\sim 2\%$ ) and can be expressed in terms of a rate of shift per per cent strain ( $d\Delta\nu/de, \text{ cm}^{-1}/\%$ ). However, such linearity was not sustained at high strains and it was found that as strain increased,  $d\Delta\nu/de$  decreased and eventually there was no further decrease in frequency with further straining (Fig. 7). This corresponds to a yielding phenomenon and it can be seen from Fig. 7 that for Fibre A the low-load-bearing band shows yielding at about 5% strain whereas the high-load-bearing band shows yielding at about 10% strain. Moreover for the low-load-bearing band, there seems to be some relaxation of stress after yield as there is a subsequent small increase in Raman frequency. The difference in yield strain shows that the

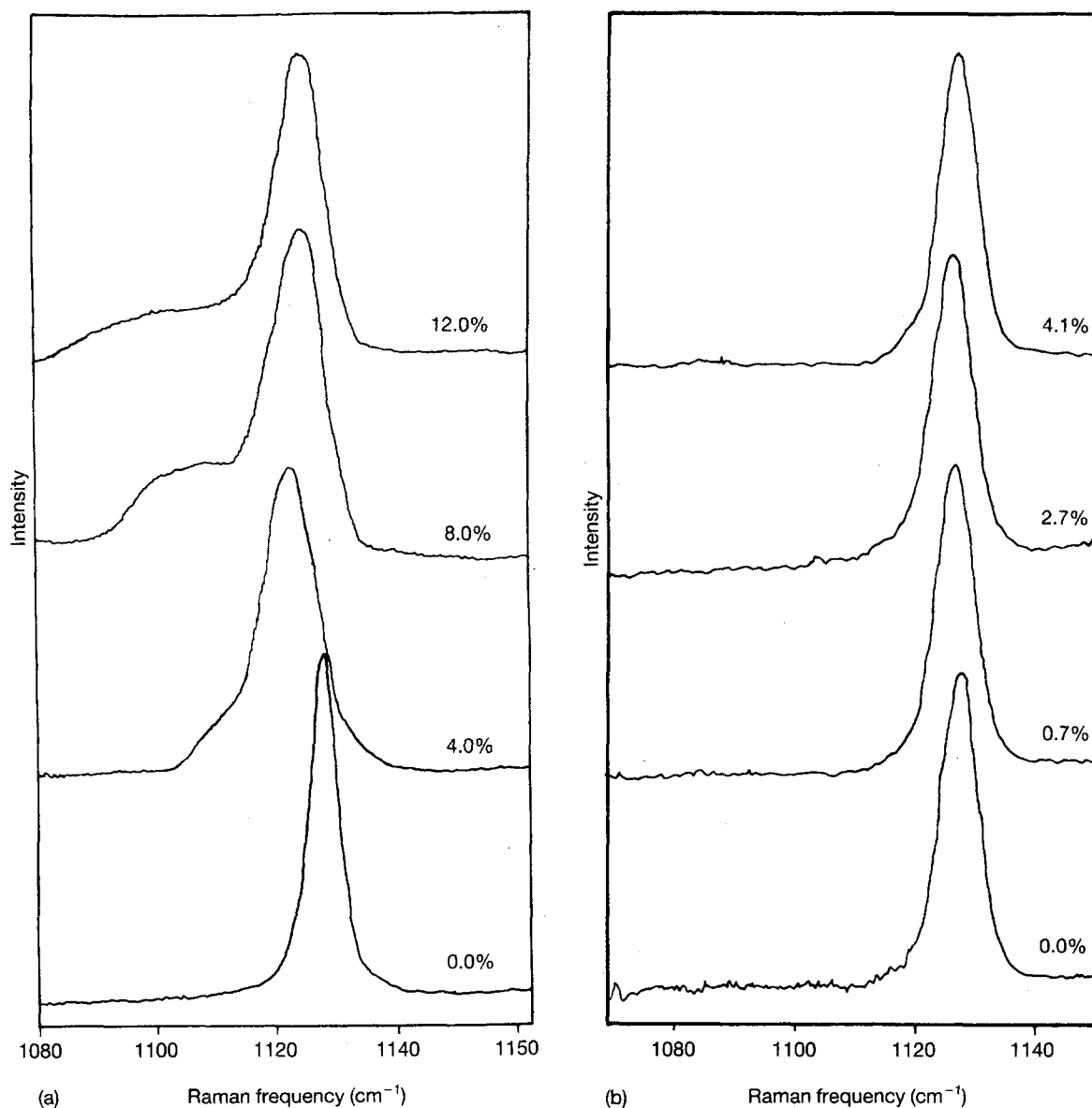


Figure 5 The Raman spectra showing the symmetric C–C stretching mode of the monofilaments following deformation at various strains for (a) Fibre A, (b) Fibre B, and (c) Fibre C.

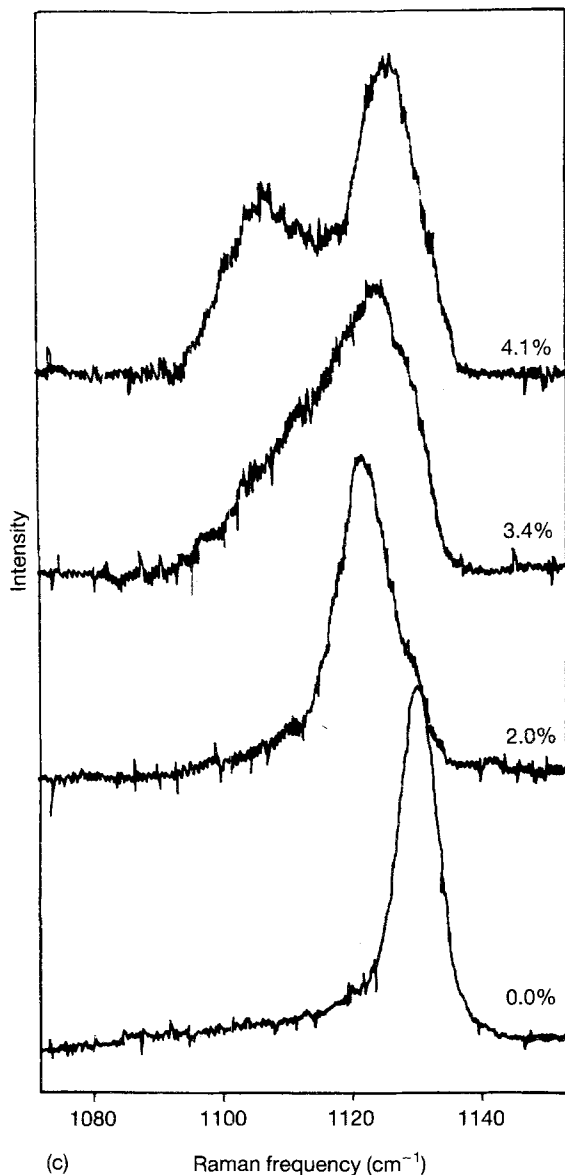


Figure 5 Continued.

two Raman bands correspond to phases in quite different microstructural environments. It should be pointed out that end effects were observed from the Raman frequency/strain curves such as Fig. 7 due to insufficiently long gauge lengths being employed. Therefore, by extrapolating to infinite gauge length, the corrected values of rate of shift ( $d\Delta\nu/de$ ) for both the low-load- and high-load-bearing C-C symmetric stretching bands can be determined. The corrected initial values of  $d\Delta\nu/de$  for all the samples derived from plots such as Fig. 7 are given in Table III together with the average relative areas of the Raman bands at low strains ( $< 2\%$ ). Fibre C shows the highest rate of shift for both the low-load- and high-load-bearing bands and it should be pointed out that this fibre also has the highest modulus (Table II).

Fig. 8 shows the variation of the average relative area of the Raman peaks at low levels of strain (2%) with the modulus of the fibres. It can be seen that for most of the fibres at this level of strain the low-load-bearing narrow peak constitutes about 60% of the Raman band with the high-load-bearing broad peak accounting for the remaining 40%, although there is

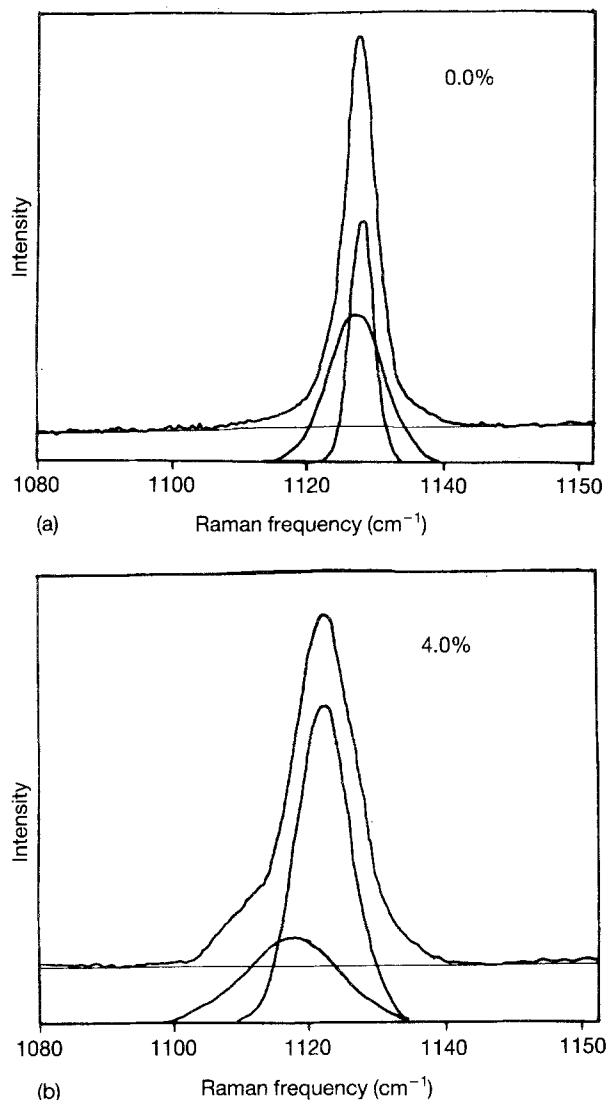


Figure 6 Raman spectra showing the symmetric C-C stretching mode for monofilaments of Fibre A at (a) 0.0%, and (b) 4.0% strains together with the two fitted Gaussian curves following background subtraction.

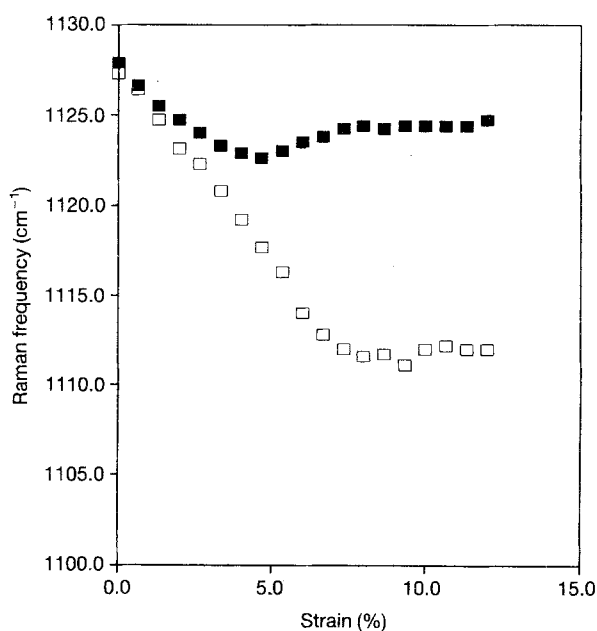


Figure 7 Raman frequency versus strain curves for monofilaments of Fibre A using a strain rate of  $1.33 \times 10^{-4} \text{ s}^{-1}$  and gauge length of 25.0 mm. (■) Narrow band, (□) broad band.

TABLE III Corrected initial values of  $d\Delta\nu/de$  and relative areas of the Raman peaks for all samples

Fibre	Corrected $d\Delta\nu/de$		Relative area	
	Low-load bearing band ( $\text{cm}^{-1}/\%$ )	High-load bearing band ( $\text{cm}^{-1}/\%$ )	Low-load bearing band	High-load bearing band
A	2.01	3.34	0.59	0.41
B	0.21	0.18	0.68	0.32
C	4.58	6.77	0.68	0.32
D	0.39	2.03	0.60	0.40
E	0.68	1.38	0.62	0.38
F	1.11	2.96	0.65	0.35
G	0.28	2.66	0.64	0.36
H	1.52	4.62	0.63	0.37
I	0.91	3.16	0.45	0.55

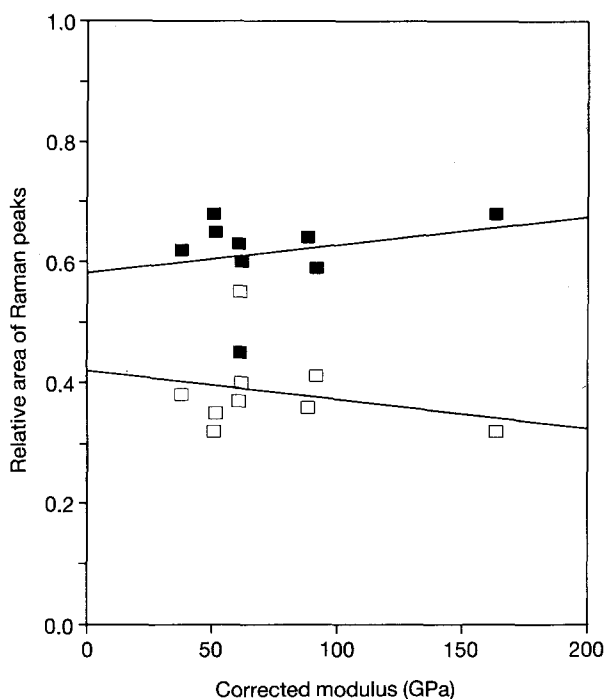


Figure 8 The variation of relative area of the Raman peaks with the corrected fibre modulus for the (■) low-load-bearing narrow and (□) high-load-bearing broad peaks.

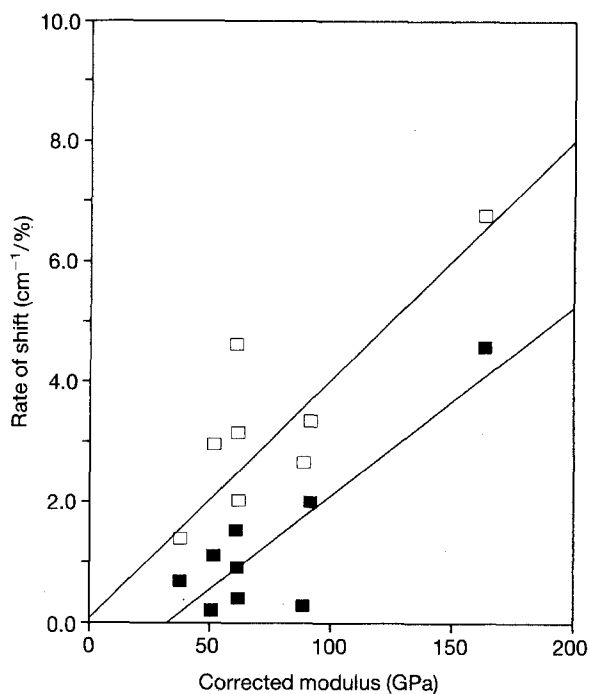


Figure 9 The variation of the rate of shift of both the (■) low-load-bearing narrow and (□) high-load-bearing broad peaks with the fibre modulus (corrected for gauge length).

considerable scatter in the data. Moreover, it was found that the relative area of the high-load-bearing broad peak increased with strain [28] especially for the higher-modulus fibres (e.g. Fig. 5c for Fibre C) showing considerable microstructural reorganization during deformation. This indicates the increasing importance of the high-load-bearing C-C bonds to the mechanical properties of the PE fibres. In addition, the rates of shift of both the narrow and broad peaks increase significantly with increasing fibre modulus as shown in Fig. 9. It appears, therefore, that both parameters may be significant in controlling the high-performance mechanical properties of the gel-spun PE fibres. It may be assumed to a first approximation that the number of low-load- and high-load-bearing C-C bonds are proportional to the areas of their respective Raman bands. If it is assumed further that the rate of shift of the individual bands is an indication of the level of molecular deformation (as in Kevlar [29]), then it is possible to combine the relative band areas  $A$

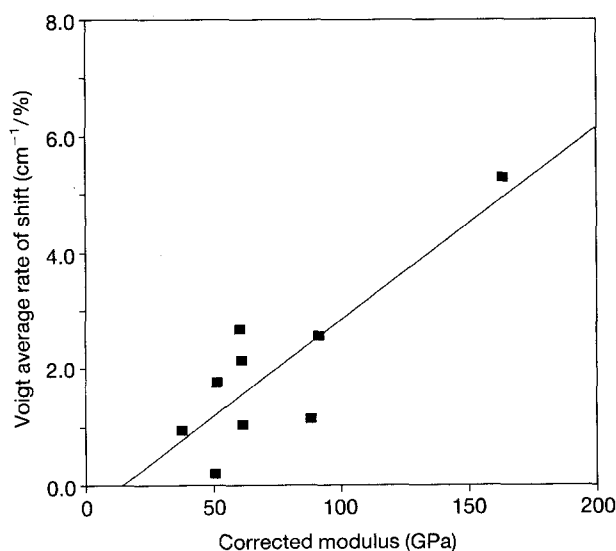


Figure 10 The variation of the average rate of peak shift (normalized for peak area) with the corrected modulus of the fibres.

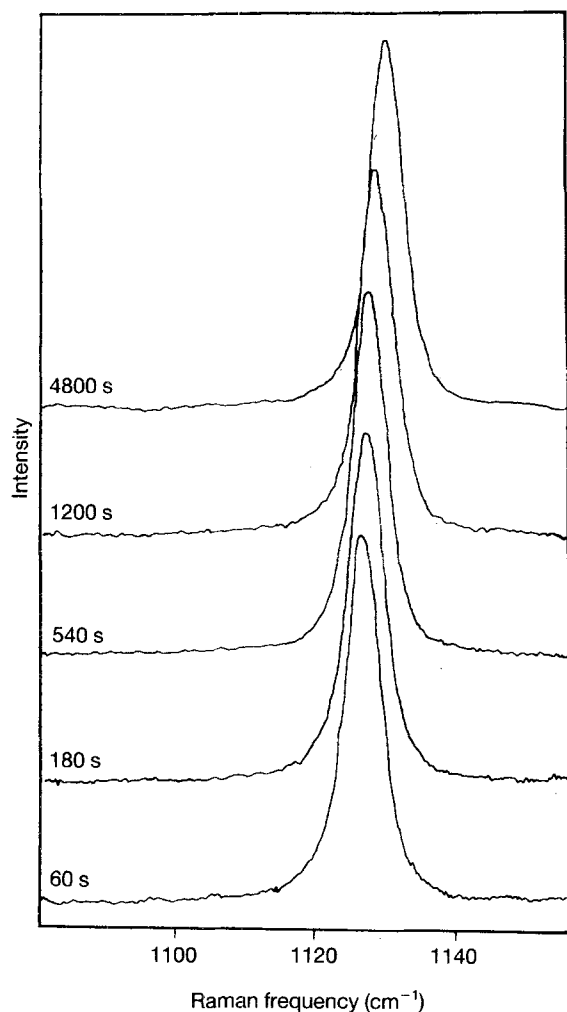


Figure 11 Change in the position of the C–C symmetric stretching Raman band with time for a monofilament of Fibre A upon stress relaxation at a constant 2.0% strain.

and rate of shift ( $d\Delta\nu/de$ ) into a single parameter which may indicate the level of overall molecular deformation in the microstructure. This can be done in the first instance assuming a “rule of mixtures” averaging process of the form

$$A_1 \left[ \frac{d\Delta\nu}{de} \right]_1 + A_2 \left[ \frac{d\Delta\nu}{de} \right]_2 \quad (1)$$

where the subscripts 1 and 2 refer to the high- and low-load-bearing bands, respectively. Fig. 10 shows the dependence of this average rate of shift parameter upon the modulus of the fibres and it can be seen that the data points fall on a line which has an intercept close to the origin. It will be shown that this information is important for the molecular interpretation of fibre deformation [30].

### 3.3. Stress relaxation and creep

Fig. 11 shows that shifts in the frequency of the Raman bands for the symmetric C–C stretching Raman mode of the monofilaments were observed during the stress relaxation of Fibre A held at a constant displacement corresponding to a 2% strain. If the Raman bands are again fitted to two Gaussian functions, a complex

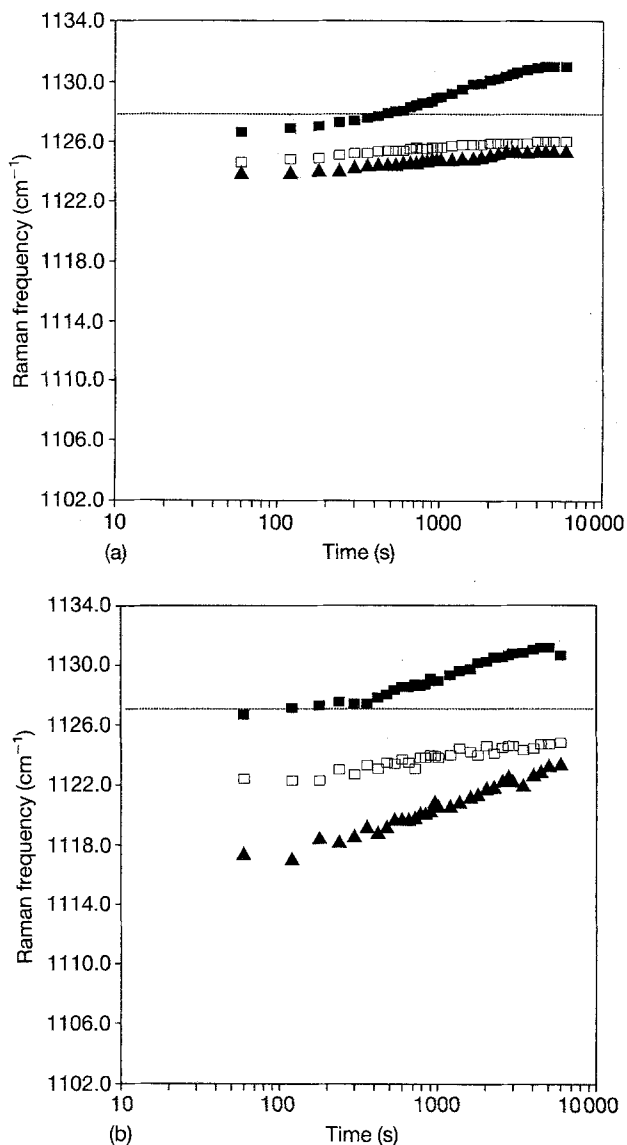


Figure 12 The Raman frequency versus time curves of both (a) low-load-, and (b) high-load-bearing bands for monofilaments of Fibre A during stress relaxation at (■) 2.0%, (□) 4.0% and (▲) 0.6% strain.

molecular behaviour is found where both the low-load (narrow) and high-load (broad) bearing bands shift towards the initial peak frequency (Fig. 12). This increase in frequency corresponds to a reduction in molecular stress and the behaviour is quite unusual. At 2.0% strain, both the low-load- and high-load-bearing C–C bonds became subjected to apparent compression (a positive shift of the Raman peak relative to the original position) after  $\sim 600$  and  $\sim 200$  s relaxation, respectively. This complex behaviour at low strain may be due to viscoelastic reorganization of the microstructure of the material but as yet remains unexplained. At higher applied strain, however, the bands always remained in tension.

Fig. 13 shows the Raman spectra of Fibre A during the creep experiments of the monofilaments at a constant stress of 0.5 GPa. Again, the peak positions of the Raman bands shift with time towards the original position even though the monofilament is under constant applied stress (Fig. 14). However, the changes in band frequency are not as significant as those during

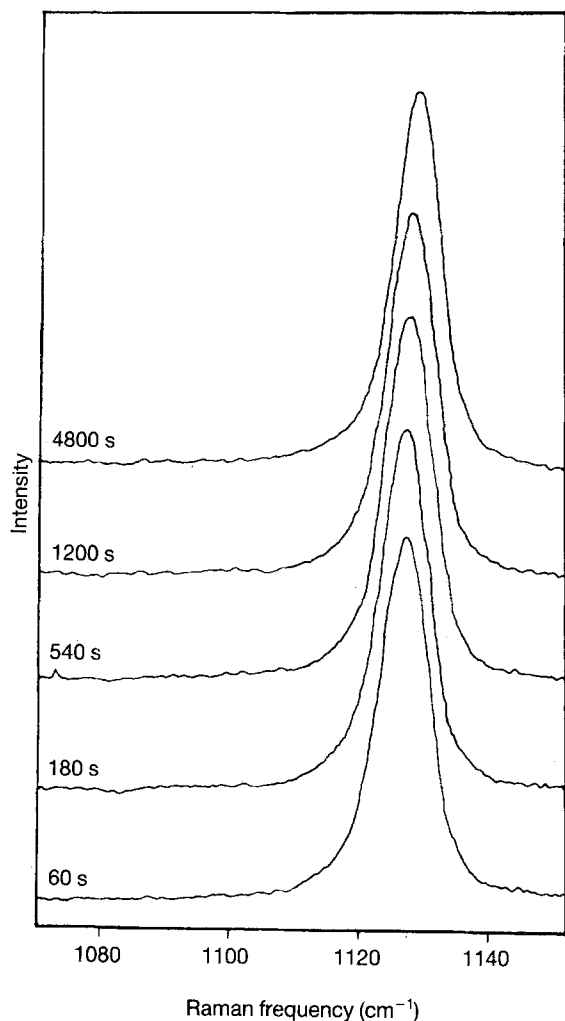


Figure 13 Change in peak position of the C-C symmetric stretching Raman band with time for a monofilament of Fibre A upon creep experiment at a constant stress of 0.5 GPa.

stress relaxation and Fig. 14 shows that only the low-load-bearing band shows a positive shift relative to the original position only at constant stresses of 0.5 and 1.5 GPa. The interpretation of such complex molecular behaviour in stress relaxation and creep will be possible using the microfibrillar model [30].

#### 4. Conclusion

There are some similarities in structure and morphology between the gel-spun and melt-spun PE fibres. These fibres show similar surface texture using FE-SEM even though they were prepared differently. However, using permanganic etching, the details of the microstructure for the fibres could be seen using TEM and the gel-spun fibres apparently show a higher degree of chain extension than the melt-spun fibres. Using the technique of Raman microscopy, it is possible to obtain a unique view of the molecular deformation processes in the PE monofilaments. Generally, gel-spun PE fibres with high-performance mechanical properties show both a high rate of Raman band shift with strain and a high intensity of the high-load-bearing Raman band during straining which are both thought to be important parameters for the molecular interpretation of fibre deformation.

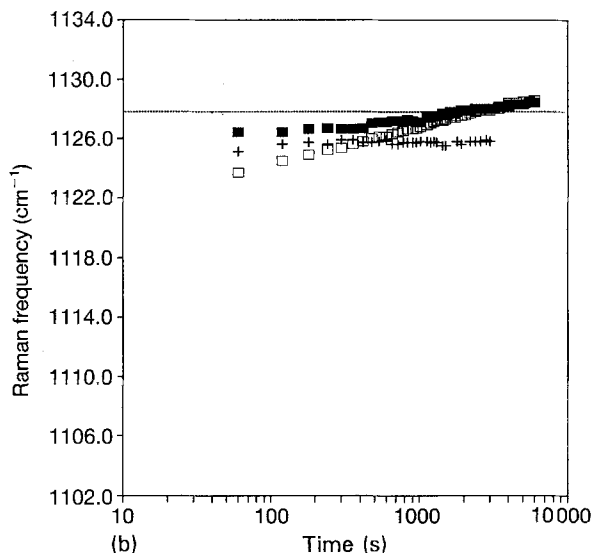
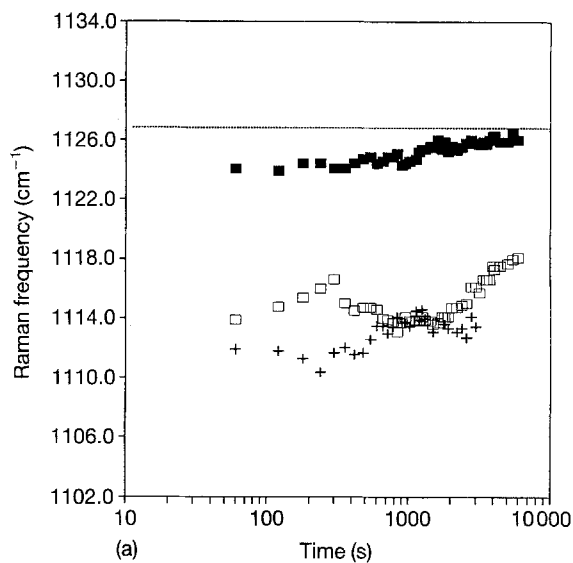


Figure 14 The Raman frequency versus time curves for (a) low-load-, and (b) high-load-bearing bands for monofilaments of Fibre A during creep experiment at constant stresses of (■) 0.5, (□) 1.5 and (+) 2.5 GPa.

This will be analysed in detail in the following paper [30].

#### Acknowledgements

The work was supported by Allied Signal Inc. who also supplied the gel-spun polyethylene fibres. The authors are grateful to Dr D. Prevorsek, Allied Signal, for useful discussion and R. J. Y. thanks the Royal Society for support in the form of the Wolfson Research Professorship in Materials Science.

#### References

1. P. J. LEMSTRA and R. KIRSCHBAUM, in "Developments in Oriented Polymers 2," edited by I. M. Ward (Elsevier Applied Science, London, 1987).
2. Allied Corp., US Pat. 4413 110.
3. Dyneema VoF Information Brochure, "Dyneema SK60: High Strength/High Modulus Fiber, Properties & Applications", (DSM, 1987).
4. Dyneema VoF Information Brochure, "Dyneema SK60: High Performance Fibers in Composites" (DSM, 1988).

5. E. H. M. VAN GORP and J. L. J. VAN DINGENEN, in "Innovative Technologies in Industrial Textiles: Textile Institute Industrial, Technical and Engineering", Textile Conferences, 5-6 February 1990.
6. K. F. MULDER, in "High Performance Plastics", August 1991, edited by A. Duckett and I. Guy (Elsevier Applied Science, Oxford) p. 1.
7. R. J. YOUNG, in "Comprehensive Polymer Science: The Synthesis, Characterization, Reactions and Applications of Polymers", Vol. 2, "Polymer Properties", edited by C. Booth and C. Price (Pergamon Press, Oxford) p. 515.
8. L. HOLLIDAY, in "Structure and Properties of Oriented Polymers", edited by I. M. Ward (Applied Science, London, 1975) p. 242.
9. V. K. MITRA, *J. Chem. Phys.* **66** (1977) 2731.
10. D. N. BATCHELDER and D. BLOOR, *J. Polym. Sci. Polym. Phys. Ed.* **17** (1979) 569.
11. C. GALIOTIS, R. J. YOUNG and D. N. BATCHELDER, *J. Polym. Sci. Polym. Phys.* **21** (1983) 2483.
12. R. J. YOUNG, in "Developments in Oriented Polymers 2", edited by I. M. Ward (Elsevier Applied Science, London, 1987) p. 1.
13. C. GALIOTIS, I. M. ROBINSON, R. J. YOUNG, B. J. E. SMITH and D. N. BATCHELDER, *Polym. Commun.* **26** (1985) 354.
14. S. van der Zwagg, M. G. NORTHOLT, R. J. YOUNG, I. M. ROBINSON, C. GALIOTIS and D. N. BATCHELDER, *ibid.* **28** (1987) 276.
15. R. J. YOUNG, D. LU and R. J. DAY, *Polym. Int.* **24** (1991) 71.
16. R. J. YOUNG, R. J. DAY and M. ZAKIKHANI, *J. Mater. Sci.* **25** (1990) 127.
17. R. J. DAY, I. M. ROBINSON, M. ZAKIKHANI and R. J. YOUNG, *Polymer* **28** (1987) 1833.
18. K. TASHIRO, G. WU and M. KOBAYASHI, *ibid.* **29** (1988) 1768.
19. K. PRASAD and D. T. GRUBB, *J. Polym. Sci. Polym. Phys. Ed.* **27** (1989) 381.
20. B. J. KIP, M. C. P. Van EIJK and R. J. MEIER *ibid.* **29** (1991) 99.
21. J. A. H. M. MOONEN, W. A. C. ROOVERS, R. J. MEIER and B. J. KIP, *J. Polym. Sci. Polym. Phys.* **30** (1992) 361.
22. D. T. GRUBB and Z. LI, *Polym.* **30** (1992) 2587.
23. Allied-Signal Inc., private communication.
24. R. G. C. ARRIDGE, P. J. BARHAM, C. J. FARRELL and A. KELLER, *J. Mater. Sci. Lett.* **11** (1976) 788.
25. D. C. BASSETT, in "Developments in Crystalline Polymers, 2", edited by D. C. Bassett (Elsevier Applied Science, London, 1988) p. 67.
26. J. BRANDRUP and G. H. IMMERGUT, "Polymer Handbook", 3rd edn (Wiley Interscience, New York, 1989).
27. D. N. BATCHELDER, *Eur. Spectrosc. News* **80** (1988) 28.
28. W. F. WONG, PhD thesis, Victoria University of Manchester, (1992).
29. R. J. YOUNG, D. LU, R. J. DAY, and W. F. KNOFF and H. A. DAVIS, *J. Mater. Sci.* **27** (1992) 5431.
30. W. F. WONG and R. J. YOUNG, *ibid.* **28** (1993) 0000.

*Received 22 February  
and accepted 20 April 1993*